# Moment Method Boundary Conditions for Multiphase Lattice Boltzmann Simulations with Partially-wetted Walls

**Andreas Hantsch[1,*], Tim Reis[2] and Ulrich Gross[3]**
[1]Institute of Air Handling and Refrigeration gGmbH, Bertold-Brecht-Allee 20, 01309 Dresden, Germany
[2]School of Computing and Mathematics, Plymouth University, Plymouth, PL4 8AA, United Kingdom
[3]Institute of Thermal Engineering, Technische Universität Bergakademie Freiberg, G.-Zeuner-Str. 7, 09596 Freiberg, Germany

Received: 5 June 2014, Accepted: 19 December 2014

**Abstract**
We propose a lattice Boltzmann approach for simulating contact angle phenomena in multiphase fluid systems. Boundary conditions for partially-wetted walls are introduced using the moment method. The algorithm with our boundary conditions allows for a maximum density ratio of 200000 for neutral wetting. The achievable density ratio decreases as the contact angle departs from 90°, but remains of the order $\mathcal{O}(10^2)$ for all but extreme contact angles. In all simulations an excellent agreement between the simulated and nominal contact angles is observed.

**Keywords:** Lattice Boltzmann Method, Multiphase Flow, Moment-based Boundary Conditions, Partial Wetting

## 1. INTRODUCTION

Wetting of solid structures is an interesting phenomenon in nature and also of much importance in many technical processes. For instance, in condensers it is desirable to have a large angle of contact between a liquid and solid in order to promote drop-wise, rather than film-wise, condensation [14]. The opposite is true for the case of evaporators, where a closed liquid film flow can be supported with a small contact angle. The contact angle $\theta$ can be observed at the three-phase line where solid, liquid, and vapour meet. A contact angle of $\theta = 90°$ is usually called neutral wetting. Smaller or larger angles cause mostly wetting or mostly dewetting, respectively [9].

With increasing computational resources, the numerical modelling and simulation of physical phenomena becomes more and more important. Traditional computational methods for multiphase flow are discretisations of the macroscopic equations of motion (see Prosperetti and Tryggvason [31] for a review). A relatively new method based on a mesoscopic description of a fluid, namely the lattice Boltzmann method (LBM), has been gaining prominence in recent years (for a review, see Chen and Doolen [8], Yu et al. [42], Aidun and Clausen [1]). The LBM is derived from a velocity-space truncation of the famous Boltzmann equation with a simplified collision operator [18]. Once further discretised in space-and-time, the resulting numerical algorithm may be efficiently implemented on modern parallel computer architectures [2, 10, 40]. The primary variable in the LBM is the discrete-velocity distribution function. Macroscopic quantities, such as density, momentum, and stress, are determined by taking discrete moments of the distribution function.

The first generation of multiphase lattice Boltzmann models are often referred to as "colour gradient" models [13, 33]. The interfacial dynamics are predicted using the gradient of an order parameter (the "colour") used to distinguish between the two fluids. Although improvements have been made to the original model [12, 24, 32], colour-gradient approaches can still suffer

*Corresponding author. Email: andreas.hantsch@ilkdresden.de

from numerical instabilities at high density ratios and can be computational expensive due to the necessary "recolouring" step in the algorithm. The popular pseudo-potential model of Shan and Chen [35] introduces a long-range interaction force to promote phase segregation. To improve its numerical stability, Kuzmin et al. [23] extended the Shan-Chen model from a single- to a multiple-relaxation time algorithm, and Sun et al. [37] have performed an investigation into the accuracy of the equation of state in the model. Despite further enhancements to reduce so-called spurious currents and increase the attainable density ratio [11, 34], the model remains thermo-dynamically inconsistent, as has been demonstrated by Swift et al. [38] and He and Doolen [15]. Motivated by this, Swift et al. [38] introduced their free-energy lattice Boltzmann equation, which employs a Cahn-Hilliard equation for phase dynamics. Although the original formulation lacks Galilean invariance, this may be restored by adding a correction term into the equilibrium distribution function [20]. A major extension of the model was provided by Inamuro et al. [21], who were the first to present a multiphase lattice Boltzmann model capable of simulating flows with a density ratio of the order of $10^3$. This was achieved by forcing exact incompressibility of both phases, but came at the cost of calculating the pressure iteratively via a separate Poisson equation. Like other models, free-energy LBMs suffer from parasitic currents in the vicinity of an interface. Wagner [39] argued that these are due to inconsistent discretisations of the forcing terms and found that using a potential form of the surface tension term (instead of a pressure form) dramatically reduces these spurious phenomena. Further progress was made by Jamet et al. [22] before a consistent and isotropic lattice Boltzmann discretisation was proposed by Lee and Fischer [26]. Despite the novelty and success of the Lee-Fischer model, it has some difficulty in incorporating macroscopically consistent boundary conditions [25, 27, 28, 41]. For example, bounce-back conditions must be applied halfway between nodes in order to achieve second-order accuracy [16]. Furthermore, numerical slip errors due to the combination of bounce-back and a single relaxation time collision operator increase with the lattice viscosity, requiring a highly resolved mesh for low Reynolds number flow. This adds additional complications to multiphase LBMs which usually impose contact angle conditions at a wall.

In this paper we propose a new approach to model partially-wetted walls with lattice Boltzmann methods. We combine two approaches, namely moment method [4] and free-energy boundary conditions for multiphase flow [5, 6]. This new wall boundary condition may be employed, in principle, for a variety of multiphase or multi-component lattice Boltzmann models.

## 2. NUMERICAL MODEL

### 2.1 Multiphase Lattice Boltzmann equation model

We employ the Lee-Fischer model [26], which has followed from the contributions of He et al. [19], Jamet et al. [22], and Wagner [39]. Its most remarkable features are its ability to attain large density ratios and greatly reduced spurious currents at the liquid-vapour interface.

The Lee-Fischer model is obtained from a Crank-Nicolson discretisation of the discrete-velocity Boltzmann equation for distribution functions $f_q = f_q(\boldsymbol{x},\ \boldsymbol{e}_q, t)$ with an interface forcing term. The resulting algorithm may be written as [19, 26]:

$$\overline{f}_q(\boldsymbol{x} + \boldsymbol{e}_q\Delta t, t + \Delta t) - \overline{f}_q(\boldsymbol{x}, t) = \mathcal{C}_q + \mathcal{F}_q, \tag{1}$$

where the *transformed* distribution functions $\bar{f}_q$ are defined in Eq. (2). The collision term $\mathcal{C}_q$, defined in Eq. (5), relaxes $\bar{f}_q$ to its (transformed) equilibria $\overline{f}_q^{\,\mathrm{eq}}$ while the force term $\mathcal{F}_q$ (c. f. Eq. (6)) imposes the surface tension. The left-hand side of the above equation represents a perfect shift of the distribution function $\bar{f}_q$ in the direction $q$ from node $\boldsymbol{x}$ at time $t$ to a neighbouring node $\boldsymbol{x} + \boldsymbol{e}_q\Delta t$ at the new time step $t + \Delta t$. The stencil is defined by Eq. (12).

The transformed functions $\bar{f}_q$ and $\overline{f}_q^{\,\mathrm{eq}}$ depend up on $f_q$ and their equilibria $f_q^{\mathrm{eq}}$ as follows:

$$\overline{f}_q = f_q + \frac{\Delta t(f_q - f_q^{\mathrm{eq}})}{2\tau} - \frac{f_q^{\mathrm{eq}}\Delta t}{2\varrho c_{\mathrm{s}}^2}(\boldsymbol{e}_q - \boldsymbol{u})\cdot\boldsymbol{F},\ \text{and} \tag{2}$$

$$\overline{f}_q^{\mathrm{eq}} = f^{\mathrm{eq}}{}_q - \frac{f_q^{\mathrm{eq}}\Delta t}{2\varrho c_{\mathrm{s}}^2}(\boldsymbol{e}_q - \boldsymbol{u})\cdot\boldsymbol{F}, \tag{3}$$

whereby

$$f_q^{\mathrm{eq}} = w_q\varrho\left[1 + \frac{\boldsymbol{e}_q\cdot\boldsymbol{u}}{c_{\mathrm{s}}^2} + \frac{(\boldsymbol{e}_q\cdot\boldsymbol{u})^2}{2c_{\mathrm{s}}^4} + \frac{u^2}{2c_{\mathrm{s}}^2}\right] \tag{4}$$

is the equilibrium distribution function from the discrete-velocity Boltzmann equation [17]. Herein, $\boldsymbol{e}_q$ and $\boldsymbol{u}$ are the microscopic and macroscopic velocities, respectively, and the speed of sound $c_{\mathrm{s}} = 1/\sqrt{3}$ is a lattice constant.

In the model of Lee and Fischer [26], the collision term is defined by:

$$\mathcal{C}_{q,\mathrm{SRT}} = -\frac{\Delta t}{\tau + 0.5\Delta t}(\overline{f}_q - \overline{f}_q^{\mathrm{eq}}), \tag{5}$$

utilising a single-relaxation time $\tau$ (SRT). The force term $\mathcal{F}_q$ can be expressed as [26]:

$$\mathcal{F}_q = \frac{(\boldsymbol{e}_q - \boldsymbol{u})\cdot\boldsymbol{F}}{\varrho c_{\mathrm{s}}^2} f_q^{\mathrm{eq}}\Delta t, \tag{6}$$

and the force vector by

$$\boldsymbol{F} = c_{\mathrm{s}}^2\boldsymbol{\nabla}\varrho - \varrho\boldsymbol{\nabla}\mu, \tag{7}$$

where $\mu$ is the chemical potential (defined in Eq. (22)), and $\varrho$ is the mass density. We follow Lee and Fischer [26] and discretise the gradient terms in Eqs. (2), (3), and (6) using both central and upwind schemes. More specifically, the directional derivatives of the form $\boldsymbol{e}_q\cdot\nabla\chi$ for some scalar $\chi$ in Eq. (6) require the mixed difference scheme

$$\boldsymbol{e}_q\cdot\nabla\chi = \frac{1}{2}\left[\frac{\chi(\mathbf{x}+\boldsymbol{e}_q\Delta t) - \chi(\mathbf{x}-\boldsymbol{e}_q\Delta t)}{2\Delta t} + \frac{-\chi(\mathbf{x}+2\boldsymbol{e}_q\Delta t) + 4\chi(\mathbf{x}+\boldsymbol{e}_q\Delta t) - 3\chi(\mathbf{x})}{2\Delta t}\right]. \tag{8}$$

The directional derivatives in Eqs. (2) and (3) are approximated by

$$\boldsymbol{e}_q\cdot\nabla\chi = \frac{\chi(\mathbf{x}+\boldsymbol{e}_q\Delta t) - \chi(\mathbf{x}-\boldsymbol{e}_q\Delta t)}{2\Delta t}, \tag{9}$$

and the remaining first and second order derivatives in Eqs (2), (3), and (6) are computed using the central differences

$$\nabla\chi = \sum_q \frac{w_q\boldsymbol{e}_q\left[\chi(\mathbf{x}+\boldsymbol{e}_q\Delta t) - \chi(\mathbf{x}-\boldsymbol{e}_q\Delta t)\right]}{2c_s^2\Delta t} \tag{10}$$

$$\nabla^2\chi = \sum_q \frac{w_q\left[\chi(\mathbf{x}+\boldsymbol{e}_q\Delta t) - 2\chi(\mathbf{x}) - \chi(\mathbf{x}-\boldsymbol{e}_q\Delta t)\right]}{c_s^2\Delta t^2}. \tag{11}$$

A detailed discussion of the need for compact gradient discretisation can be found in [26, 29]. We consider a 9-point lattice with microscopic velocities

$$\boldsymbol{e}_q = \begin{cases} (0,0)^{\mathrm{T}}, & q = 0 \\ (\cos[0.5(q-1)\pi],\ \sin[0.5(q-1)\pi])^{\mathrm{T}}, & 1 \le q \le 4 \\ (\cos[0.5(q-5)\pi + 0.25\pi],\ \sin[0.5(q-5)\,\pi + 0.25\pi])^{\mathrm{T}}, & 5 \le q \le 8, \end{cases} \tag{12}$$

where T denotes transpose, and weighting factors

$$w_q = \begin{cases} 4/9, & q = 0 \\ 1/9, & 1 \le q \le 4 \\ 1/36, & 5 \le q \le 8. \end{cases} \tag{13}$$

The hydrodynamic quantities are obtained via discrete moments of the transformed distribution functions. For example, the mass and momentum are computed from

$$\varrho = \sum_q \overline{f}_q^{\mathrm{eq}} = \sum_q \overline{f}_q, \text{ and} \tag{14}$$

$$\varrho \boldsymbol{u} = \sum_q \boldsymbol{e}_q \overline{f}_q^{\mathrm{eq}} + \frac{\Delta t}{2}\boldsymbol{F} = \sum_q \boldsymbol{e}_q \overline{f}_q + \frac{\Delta t}{2}\boldsymbol{F}. \tag{15}$$

By performing a Chapman-Enskog expansion (see, e.g., Chapman and Cowling [7]) it can be shown that the Lee-Fischer lattice Boltzmann equation approximates the following equations of motion for mass and momentum in the macroscopic limit:

$$\partial_t \varrho + \boldsymbol{\nabla}\cdot(\varrho \boldsymbol{u}) = 0, \tag{16a}$$

$$\partial_t(\varrho \boldsymbol{u}) + \boldsymbol{\nabla}\cdot(\varrho \boldsymbol{u}\boldsymbol{u}) = -\boldsymbol{\nabla} p + \boldsymbol{\nabla}\cdot\left[\eta(\boldsymbol{\nabla}\boldsymbol{u} + (\boldsymbol{\nabla}\boldsymbol{u})^T)\right] + \boldsymbol{F} + \mathcal{O}(\mathrm{Ma}^3), \tag{16b}$$

where $\eta$ is the dynamic viscosity and is a function of the relaxation time $\tau$: $\eta = \varrho c_s^2 \tau$. The Mach number is $\mathrm{Ma} = u/c_s << 1$.

## 2.2 Boundary condition model

Boundary conditions are vital for all numerical methods. For the lattice Boltzmann algorithm we must supply (for a flat boundary) three incoming distributions, $\bar{f}_q$ (not necessarily $f_q$), where $\boldsymbol{e}_q$ points into the fluid. It is common, and seemingly natural, to impose boundary conditions directly upon these distribution functions (as is the case for bounce-back, for example). Alternatively, we may take advantage of the invertible relationship between the velocity basis and the moment basis. Now we can consider applying boundary conditions to the *moments* of the velocity distribution function and then translating these into conditions for the incoming $\bar{f}_q$. Imposing constraints upon the hydrodynamic moments (velocity, pressure, stress) allows for the exact satisfaction of the required boundary conditions (such as no-slip) precisely at grid points, and may be particularly convenient for imposing contact angles and Neumann-type boundary conditions.

### 2.2.1 Partial-wetting condition

The boundary conditions at the wall read (for details see de Gennes et al. [9] and Lee and Liu [27, 28]):

$$\boldsymbol{n}_s \cdot \boldsymbol{\nabla}\varrho_s = -\frac{\phi_1}{\kappa}, \tag{17a}$$

$$\boldsymbol{e}_q \cdot \boldsymbol{\nabla}\varrho_\mathrm{s} = 0, \tag{17b}$$

$$\boldsymbol{e}_q \cdot \boldsymbol{\nabla}\mu_\mathrm{s} = 0, \tag{17c}$$

where $\boldsymbol{n}_\mathrm{s}$ denotes the normal to the solid surface. Equations (17b) and (17c) ensure no flux through the solid surface, whereas Eq. (17a) determines the contact angle. It shall be stressed that Lee and Liu [27] utilised the density $\varrho$ as a phase index in a single-component two-phase flow. Lee and Liu [28], however, proposed the same equation for a binary fluid, but with the phase index $\varphi$ instead of the density $\varrho$.

The other variables in equations (17) are the surface tension parameters $\phi_1$ and $\kappa$, which can be determined with

$$\phi_1 = \frac{\Omega}{4}(\varrho_\mathrm{l} - \varrho_\mathrm{v})^2\sqrt{2\kappa\beta}, \tag{18}$$

$$\kappa = \frac{3\sigma\xi}{2(\varrho_\mathrm{l} - \varrho_\mathrm{v})^2}, \text{ and} \tag{19}$$

$$\beta = \frac{12\sigma}{\xi(\varrho_\mathrm{l} - \varrho_\mathrm{v})^4}. \tag{20}$$

Herein, $\varrho_\mathrm{l}$ and $\varrho_\mathrm{v}$ are the saturation liquid and vapour densities, respectively, $\sigma$ is the interfacial tension, $\xi$ is the interfacial width, and $\beta$ is a compressibility factor. The non-dimensional wetting potential $\Omega$ can be evaluated with

$$\Omega = 2\,\mathrm{sgn}\left(\frac{\pi}{2} - \theta_\mathrm{eq}\right)\left\{\cos\left(\frac{\alpha}{3}\right)\left[1 - \cos\left(\frac{\alpha}{3}\right)\right]\right\}^{1/2}, \tag{21}$$

and $\cos\,\alpha = (\sin\theta_\mathrm{eq})^2$, $\theta_\mathrm{eq}$ being the contact angle at equilibrium. The function sgn returns the sign of its argument.

Unlike the gradient conditions (17b) and (17c), which have to be applied to all derivatives in the forces term (7), the condition (17a) is applied in the interface term of the chemical potential only:

$$\mu = \mu_\mathrm{b} + \mu_\mathrm{int} + \mu_\mathrm{A} = \mu_\mathrm{b} - \kappa\nabla^2\varrho + \mu_\mathrm{A}. \tag{22}$$

The terms $\mu_\mathrm{b}$, $\mu_\mathrm{int}$, and $\mu_\mathrm{A}$ are those of the bulk phases, the interface, and artificial chemical potential, respectively. The interface term (2nd term in Eq. (22)) is discretised in the same manner as Lee and Liu [28]. That is, we use the stencil Eq. (11) and for nodes $\mathbf{x} + \boldsymbol{e}_q\Delta t$ outside of the computational domain we use the approximation $\chi(\mathbf{x} + \boldsymbol{e}_q\Delta t) = \chi(\mathbf{x} - \boldsymbol{e}_q\Delta t)$. The artificial chemical potential has been introduced into a binary-fluid model in order to increase the stability of the numerical scheme and reads [28]:

$$\mu_\mathrm{A} = \begin{cases} 2\beta_\mathrm{A}\varphi, & \text{for} \quad \varphi < 0 \\ 0, & \text{else,} \end{cases} \tag{23}$$

wherein $\varphi = (\varrho - \varrho_\mathrm{v})/(\varrho_\mathrm{l} - \varrho_\mathrm{v})$ is the phase index. It shall be stressed that the artificial chemical potential acts in cases of spuriously low densities only. In order to utilise the stabilising effect of the artificial chemical potential in the Lee-Fischer model, where $\beta$ and $\beta_\mathrm{A}$ are defined differently, an alternative form of $\mu_\mathrm{A}$, one with the correct units, is proposed:

$$\mu_\mathrm{A} = 2\beta_A\varphi\,(\varrho_\mathrm{l} - \varrho_\mathrm{v})^3 \quad \text{for} \;\; \varphi < 0. \tag{24}$$

### 2.2.2 Moment method boundary condition

The moment method is a general methodology for imposing macroscopic boundary conditions within the lattice Boltzmann framework. As an extension of the work by Noble et al. [30], Bennett [3] suggests finding appropriate boundary conditions for the unknown (or "incoming") distribution functions by imposing hydrodynamic boundary conditions directly upon physically meaningful moments of $f_q$. For a typical two-dimensional lattice with nine velocity directions (see Fig. 1 for a visualisation at a south wall), the hydrodynamic moments of density, momentum and momentum flux are given by

$$\begin{aligned}\Pi_0 &= \varrho \\ &= f_0 + f_1 + f_2 + f_3 + f_4 + f_5 + f_6 + f_7 + f_8,\end{aligned} \tag{25a}$$

$$\begin{aligned}\Pi_x &= \varrho u_x \\ &= f_1 - f_3 + f_5 - f_6 - f_7 + f_8,\end{aligned} \tag{25b}$$

$$\begin{aligned}\Pi_y &= \varrho u_y \\ &= f_2 - f_4 + f_5 + f_6 - f_7 - f_8,\end{aligned} \tag{25c}$$

$$\begin{aligned}\Pi_{xx} &= p + \varrho u_x u_x - 2\eta\, \partial_x u_x + \mathcal{O}(\tau^2) \\ &= f_1 + f_3 + f_5 + f_6 + f_7 + f_8,\end{aligned} \tag{25d}$$

$$\begin{aligned}\Pi_{xy} &= \varrho u_x u_y - \eta(\partial_x u_y + \partial_y u_x) + \mathcal{O}(\tau^2) \\ &= f_5 - f_6 + f_7 - f_8,\end{aligned} \tag{25e}$$

$$\begin{aligned}\Pi_{yy} &= p + \varrho u_y u_y - 2\eta\, \partial_y u_y + \mathcal{O}(\tau^2) \\ &= f_2 + f_4 + f_5 + f_6 + f_7 + f_8,\end{aligned} \tag{25f}$$

where the pressure $p$ is the ideal gas pressure: $p = c_s^2 \varrho$. The aim is to apply boundary conditions consistent with the macroscopic equations of motion to a subset of the above equations.

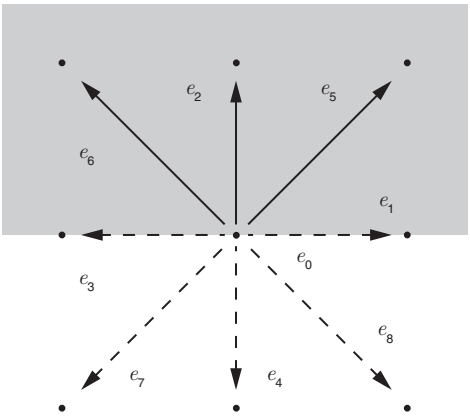


Figure 1: Two-dimensional lattice stencil with nine velocity directions (D2Q9); unknown incoming distribution functions (solid lines) at the south boundary of a computational domain (grey box).

**Table 1. Moment groups for plane horizontal boundary conditions (BC) with corresponding unknown distribution functions (adopted from [3])**

| South BC | North BC | Moments |
|---|---|---|
| $f_2+f_5+f_6$ | $f_4+f_7+f_8$ | $\Pi_0, \Pi_y, \Pi_{yy}$ |
| $f_5-f_6$ | $f_8-f_7$ | $\Pi_x, \Pi_{xy}$ |
| $f_5+f_6$ | $f_7+f_8$ | $\Pi_{xx}$ |

At a flat boundary aligned with grid points, these moments can be grouped together according to combinations of the incoming (unknown) distribution functions (see Tab. 1 for an example at a southern boundary). There are three incoming $f_q$ at such a boundary, thus we require three linearly independent equations. Moments in different groups are linearly independent. Therefore, to find the three unknown distribution functions at a flat boundary, we can pick one moment from each group, impose a constraint (boundary condition) upon each, and then solve for the incoming variables. We wish to impose no-slip and no tangential stress conditions at a solid wall (the appropriate tangential stress boundary conditions for a Newtonian fluid), so it is suggested to select $\Pi_x$, $\Pi_y$, and $\Pi_{TT}$, where $TT$ denotes the component tangential to the wall. The no-slip condition dictates $\Pi_x = \Pi_y = 0$ and the zero tangential momentum flux condition says $\Pi_{TT} = \Pi_{TT}^{\mathrm{eq}} = p$, by Eq. (25d).

However, the fully discrete lattice Boltzmann algorithm used here, Eq. (1), is in terms of $\bar{f}_q$, not $f_q$. The aim is to supply boundary conditions for $\bar{f}_q$ that are consistent with the conditions imposed upon the hydrodynamic moments, as discussed above. In other words, we have to respect the variable transformation given by Eq. (2). By taking the first order moment of Eq. (2) and imposing the zero-velocity conditions on $\Pi_x$ and $\Pi_y$ we see that the boundary conditions for $\overline{\Pi}_x$ and $\overline{\Pi}_y$ are

$$\begin{aligned}\overline{\Pi}_\alpha &= \sum_q \overline{f}_q e_{q,\alpha} \\ &= \sum_q f_q e_{q,\alpha} + \frac{\Delta t}{2\tau}\sum_q (f_q - f_q^{\mathrm{eq}}) e_{q,\alpha} - \frac{\Delta t}{2\varrho c_s^2}\sum_q (e_{q,\beta} - u_\beta) F_\beta \, e_{q,\alpha} \qquad (26)\\ &= -\Delta t F_\alpha \,/\, 2 \qquad (27)\end{aligned}$$

for $\alpha, \beta \in \{x, y\}$. Note that we have used Einstein's summing convection for repeated indices. Similarly, taking the second order moment of Eq. (2) and imposing the zero tangential stress condition $\Pi_{TT} = \Pi_{TT}^{\mathrm{eq}} = p$ shows, conveniently, that $\overline{\Pi}_{TT} = \Pi_{TT}^{\mathrm{eq}} = p$. Solving the system of equations which result from these three "barred" moments and their constraints at a south wall leads to:

$$\overline{f}_2 = \overline{f}_1 + \overline{f}_3 + \overline{f}_4 + 2(\overline{f}_7 + \overline{f}_8) - \overline{\Pi}_{xx} - 1/2\,\Delta t F_y \qquad (28a)$$

$$\overline{f}_5 = -\overline{f}_1 - \overline{f}_8 + 1/2\left[p - 1/2\,\Delta t F_x\right], \qquad (28b)$$

$$\overline{f}_6 = \overline{f}_3 + \overline{f}_7 + 1/2\left[-p - 1/2\,\Delta t F_x\right], \qquad (28c)$$

where $\varrho$ at the wall can be found in terms of known distributions:

$$\varrho = \overline{\varrho} = \sum_q \overline{f}_q \qquad (28d)$$

$$= \overline{\Pi}_y + \overline{f}_0 + \overline{f}_1 + \overline{f}_3 + 2(\overline{f}_4 + \overline{f}_7 + \overline{f}_8) \qquad (28e)$$

$$= \overline{f}_0 + \overline{f}_1 + \overline{f}_3 + 2(\overline{f}_4 + \overline{f}_7 + \overline{f}_8) - 1/2\,\Delta t F_y. \qquad (28f)$$

In a similar manner it is possible to derive the corresponding equations for a north wall.

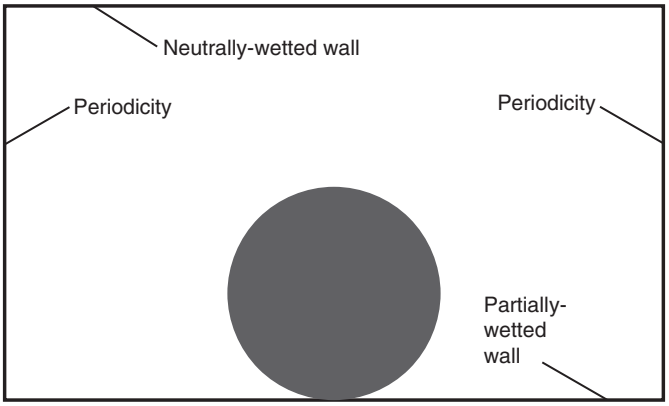


Figure 2: Geometrical representation of the computational domain and the initialisation of the drop close to the wall (indicated by grey circle, not to scale).

### 2.3 Numerical test case

The test case which has been employed here is a liquid drop close to the wall (see Fig. 2). The computational domain is rectangular with $L_y = 3/5 L_x = 5\ R_0$ and discretised with a uniform grid. The boundary condition at the north and south no-slip walls are modelled with the moment method as introduced in Sec. 2.2.2. Periodicity is implemented at the east and west boundaries. The domain is initialised with a zero-velocity field and with

$$\varrho(\boldsymbol{x}) = \frac{\varrho_\mathrm{v} + \varrho_\mathrm{l}}{2} + \frac{\varrho_\mathrm{v} - \varrho_\mathrm{l}}{2} \tanh\left( \frac{2}{\xi\left[\sqrt{(x - 1/2\, L_x)^2 + (y - R_0)^2} - R_0\right]} \right), \tag{29}$$

representing a circle with a smooth transition from liquid to vapour density of the initial radius $R_0$, whose mass centre is located at $\boldsymbol{x} = (½L_x,\ R_0)^\mathrm{T}$ and whose interface width is $\xi$. The density distribution functions have been initialised with the equilibrium distribution function.

The scaling of this system is carried out with the density ratio $\varrho^*$, the non-dimensional time and contact angle $t^*$ and $\theta^*$, respectively and the ratio of artificial to "normal" compressibility $\beta_\mathrm{A}/\beta$, utilising $t_\mathrm{sc} = \varrho_\mathrm{l} \nu_\mathrm{l} L_\mathrm{sc}/\sigma$, $\theta_\mathrm{sc} = \pi$, and $L_\mathrm{sc} = R_0$. The initial radius is varied as $R_0 \in \{20, 50\}$ (i. e., grid sizes of $100 \times 166$ and $250 \times 416$), the density ratio $\varrho^* \in \{2, 5, 7,10, 20, 50, 70, ..., 1000000\}$, the nominal contact angle $\theta^*_\mathrm{n} \in \{1/36, 1/12, 1/6, 1/4, 1/3, 1/2, 2/3, 3/4, 5/6, 11/12, 35/36\}$, and the ratio of compressibilities $\beta_\mathrm{A}/\beta \in \{0, 1, 10, 100, 1000, 2000\}$.

The kinematic viscosity $\nu$, interfacial tension $\sigma$, and interfacial width $\xi$ are set to 1/6, 0.002, and 4 in lattice units, respectively.

## 3. RESULTS AND DISCUSSION

### 3.1 Grid independence test

The test for grid independence has been carried out for two different initial drop resolutions and corresponding grid sizes. The results are illustrated in Fig. 3 in terms of actual (measured) versus nominal non-dimensional contact angle ($\theta^* \in \{1/36, 1/6, 1/2, 5/6, 35/36\}$ are tested here). Sub-figure 3(a) presents the results for $\varrho^* = 10$ and (b) for $\varrho^* = 100$. It can be observed that the solution is grid-independent as long as the simulation is numerically stable (missing symbols indicate numerical instability). A discussion of numerical stability and its influencing factors is provided below. However, it is already clear that the largest contact angle can be obtained only with the larger grid.

### 3.2 Stabilising effects of the artificial chemical potential and the collision operators

In order to study the effect of the artificial chemical potential (through the artificial compressibility $\beta_\mathrm{A}$), the results of various simulations are plotted in terms of actual versus nominal non-dimensional contact

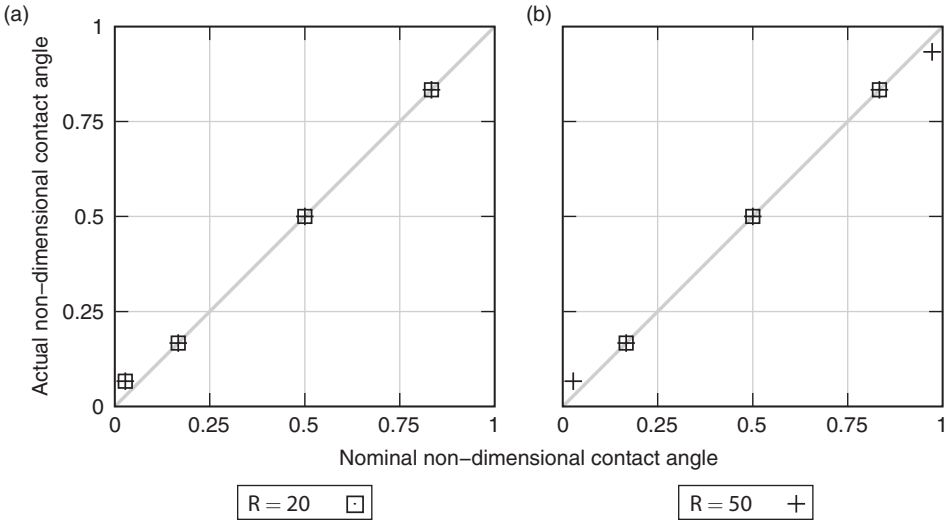


Figure 3: Grid independence test for $\varrho^* = 10$ (a) and $\varrho^* = 100$ (b) with $\beta_A/\beta = 100$, and various numbers of grid points within the initial drop radius.

angle in Fig. 4. The density ratios are 10 (a), 200 (b), and 1000 (c). It is stressed that missing symbols indicate numerically unstable simulations. An excellent agreement is observed in all but the most extreme contact angles. The range of stable contact angles is certainly sufficient for most industrial applications. It is worth mentioning that previous works could not even achieve extreme contact angles [5, 6, 27, 36, 41]. For very large density ratios it can be observed that the range of numerically stable contact angles becomes smaller, whereby it shall be noted that neutral wetting remains stable for all artificial compressibilities at larger density ratios.

The stabilising effect of the artificial compressibility is visualised in Fig. 5, which plots the maximum density ratio versus the nominal non-dimensional contact angle. The parameter is the artificial compressibility $\beta_A$. It can be observed that it is possible to employ the boundary condition proposed here for density ratios up to 200 for all contact angles under investigation. For cases of less extreme contact angles, the density ratio can exceed 1000, and for neutral wetting this can be increased to 200000. The latter fact is quite surprising, especially considering such a large density ratio has not been demonstrated for a multi-phase lattice Boltzmann model with wall boundary conditions, to the best of the authors' knowledge. As already learned from Fig. 4, there is a lower limit for stable simulations with large artificial compressibilities. The stability range for $\beta_A/\beta = 2000$ is illustrated by the grey colour. The lower limit for $\beta_A/\beta = 100$ is $\varrho^* = 10$, which has not been illustrated here in order to keep the figure clear. Hence, it is suggested to chose the numerical value of $\beta_A$ depending upon the density ratio in order to obtain optimal stability conditions. These results suggest the following heuristic conditions:

$$\frac{\beta_A}{\beta} = \begin{cases} 0, & \text{for} \quad \varrho^\star < 10 \\ 100, & \text{for} \quad 10 \leq \varrho^\star < 100 \\ 2000, & \text{for} \quad 100 \leq \varrho^\star < \varrho^\star_{\max} \,. \end{cases} \tag{30}$$

### 3.3 Temporal development of the velocity field

The temporal development of the maximum non-dimensional velocity for test cases with a density ratio of 100 is visualised in Fig. 6. It can be observed that the velocity decreases and approaches a finite asymptotic limit. However, for practical flow applications, where the average flow non-dimensional flow velocity is of the order of $10^{-2}$, these numbers are more than eight orders of magnitude lower. Shih et al. [36] reported non-dimensional spurious currents of the order of magnitude is of $10^{-7}$.

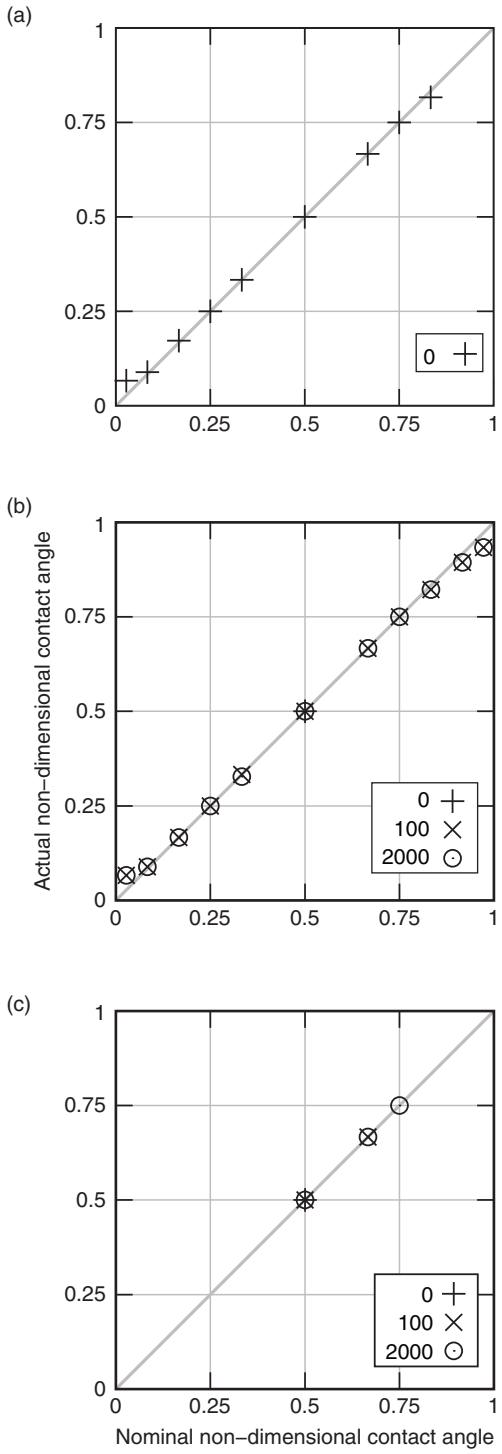


Figure 4: Actual versus nominal non-dimensional contact angle with various artificial compressibilities $\beta_{\mathrm{A}}/\beta \in \{0, 100, 2000\}$: (a) $\varrho^* = 10$, (b) $\varrho^* = 200$, (c) $\varrho^* = 1000$.

## 4. SUMMARY

A partial wetting boundary condition for the lattice Boltzmann equation method has been proposed in this contribution. It has been demonstrated that the artificial chemical potential increases the numerical stability of the system significantly. Moreover, by utilising the moment method for the unknown (incoming) distribution functions at a boundary allows us to construct consistent conditions by virtue of the physical hydrodynamic moments of the distribution functions.

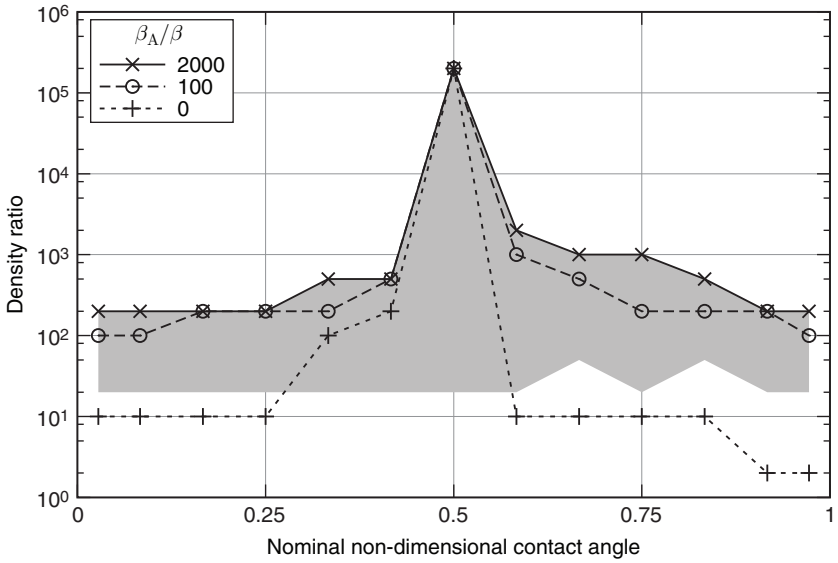


Figure 5: Maximum stable density ratio versus nominal non-dimensional contact angle with various artificial compressibilities $\beta_A$; stability range for $\beta_A/\beta = 2000$ is indicated by the grey colour; lower stability limit of $\beta_A/\beta = 100$ is $\varrho^* = 10$, which has not been visualised explicitly.

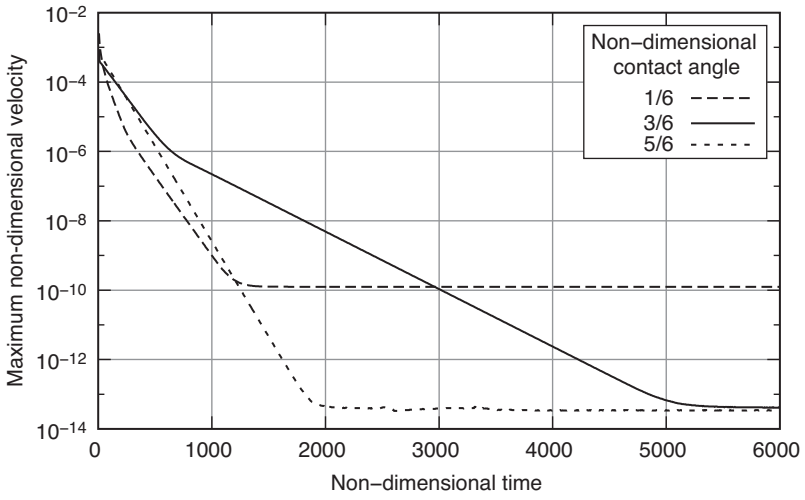


Figure 6: Temporal development of the maximum non-dimensional velocity with $\varrho^* = 100$, and various contact angles ($t_{sc} = \varrho_1 \nu_1 R_0/\sigma$ ).

Our simulations reveal an initial drop radius to interface width ratio of five is sufficiently large to obtain accurate and grid-independent, results. However, for large density ratios and low artificial compressibilities an increase in the grid resolution is required. The artificial chemical potential leads to a significantly stabilised numerical scheme and allows density ratios of up to 200 for *any* contact angle. This ratio can be increased to the order of $\mathcal{O}(10^3)$ for less extreme contact angles. More surprising still is the maximum density ratio for neutral wetting conditions, which is 200000. The model does not eliminate spurious currents entirely, but they are reasonably small in magnitude.

**ACKNOWLEDGEMENT**

The authors would like to thank Dr Paul J. Dellar, and Dr Rodrigo A. Ledesma Aguilar for fruitful discussions and collaboration. Moreover, the access to the high-performance computing facilities of the Computing Centre of Technische Universität Bergakademie Freiberg is greatly appreciated.

This paper is based on work supported in part by Award No. KUK-C1-013-04, made by King Abdullah University of Science and Technology (KAUST). The authors are very thankful for the valuable comments made by the unknown reviewers.

## NOMENCLATURE

| Symbol | Meaning | Unit |
|---|---|---|
| ***Latin symbols*** | | |
| $c_s$ | speed of sound in LB units | lu/ts |
| $\mathcal{C}_q$ | collision term | |
| $\boldsymbol{e}_q$ | microscopic velocity vector in LB units: $\boldsymbol{e}_q \in \mathbb{V}$ | lu/ts |
| $f, \bar{f}$ | density distribution function, modified distribution function | kg/m$^3$ |
| $\boldsymbol{F}$ | force | N |
| $\mathcal{F}_q$ | force term | |
| $L$ | length | m |
| $\boldsymbol{n}$ | unit normal vector | |
| $p$ | pressure | N/m$^2$ |
| $q$, $Q$ | velocity direction with $q \in \{0, 1, ..., Q-1\}$ | |
| $R$ | radius | m |
| $t$ | time | s |
| $\boldsymbol{u}$ | velocity vector: $\boldsymbol{u} = (u_x, u_y, u_z)^{\mathrm{T}}$ | m/s |
| $w_q$ | weighting factors for velocity directions $q$ | |
| $\boldsymbol{x}$ | location vector: $\boldsymbol{x} = (x, y, z)^{\mathrm{T}}$ | m |
| ***Greek symbols*** | | |
| $\beta, \beta_{\mathrm{A}}$ | compressibility, artificial compressibility | Nm$^{10}$/kg$^4$ |
| $\eta$ | dynamic viscosity | kg/(ms) |
| $\theta$ | contact angle | rad |
| $\kappa$ | interfacial tension parameter | $Nm^6/kg^2$ |
| $\mu$ | chemical potential | J/mol |
| $\nu$ | kinematic viscosity | m$^2$/s |
| $\prod_i$ | moment of a distribution function with $i \in \{0, \alpha, \beta, ...\}$ | |
| $\xi$ | interface width | m |
| $\varrho$ | density | kg/m$^3$ |
| $\sigma$ | interfacial tension | N/m |
| $\tau$ | relaxation time in LB units | ts |
| $\varphi$ | phase index | |
| $\chi$ | general variable: $\chi \in \{\varrho, \mu\}$ | |
| ***Subscripts*** | | |
| 0 | initial | |
| b | bulk | |
| l | liquid | |
| s | solid | |
| sc | scaling value | |
| th | theory | |
| v | vapour | |
| ***Superscripts*** | | |
| * | non-dimensional quantity | |
| eq | equilibrium | |
| T | transpose | |
| ***Acronyms*** | | |
| LBM | lattice Boltzmann method | |
| SRT | single-relaxation time | |

## REFERENCES


[1] C.K. Aidun and J.R. Clausen. Lattice-Boltzmann method for complex flows. *Annual Review of Fluid Mechanics*, 42: 439–472, 2010.

[2] A. Banari, C. Janssen, S.T. Grilli, and M. Krafczyk. Efficient GPGPU implementation of a lattice Boltzmann model for multiphase flows with high density ratios. *Comput. Fluids*, 93: 1–17, 2014.

[3] S. Bennett. *A Lattice Boltzmann Model for Diffusion of Binary Gas Mixtures*. PhD thesis, University of Cambridge, Cambridge, 2010.

[4] S. Bennett, P. Asinari, and P.J. Dellar. A lattice Boltzmann model for diffusion of binary gas mixtures that includes diffusion slip. *Int. J. Numer. Meth. Fluids*, 69: 171–189, 2012. doi: doi: 10,1002/fld, 2549.

[5] A.J. Briant, A.J. Wagner, and J.M. Yeomans. Lattice Boltzmann simulations of contact line motion. I. Liquid-gas systems. *Phys. Rev. E*, 69(3): 031602, 2004. doi: 10.1103/PhysRevE.69.031602.

[6] A.J. Briant, P. Papatzacos, and J.M. Yeomans. Lattice Boltzmann simulations of contact line motion in a liquid-gas system. *Phil. Trans. Royal Soc.*,1:. 360(1792): 485–495, 2002.

[7] S. Chapman and T.G. Cowling. *The mathematical theory of nonuniform gases*. Cambridge University Press, Cambridge, 3 edition, 1970.

[8] S. Chen and G.D. Doolen. Lattice Boltzmann method for fluid flows. *Ann. Rev. Fluid Mechanics*, 30: 329–364, 1998. doi: 10.1146/an- nurev.fluid.30.1.329.

[9] P.-G. de Gennes, F. Brochard-Wyart, and D. Quéré, *Capillarity and Wetting Phenomena: Drops, Bubbles, Pearls, Waves*. Springer-Verlag, Berlin, Heidelberg, 2004.

[10] N. Delbosc, J.L. Summers, A.I. Khan, N. Kupur, and C.J. Noakes. Optimized implementation of the Lattice Boltzmann Method on a graphics processing unit towards real-time fluid simulation, *Comput. Math. Appl*, 67: 462–475, 2014.

[11] G. Falcucci, S. Ubertini, and S. Succi. Lattice Boltzmann simulations of phase-separating flows at large density ratios: the case of doubly attractive pseudo potentials. *Soft Matter*, 6: 4357–4365, 2010.

[12] D. Grunau, S. Chen, and K. Eggert. A lattice Boltzmann model for multiphase fluid flows. *Physics of Fluids A*, 5(10): 2557–2562, 1993.

[13] A.K. Gunstensen, D.H. Rothman, S. Zaleski, and G. Zanetti, Lattice Boltzmann model of immiscible fluids. *Phys. Rev. A*, 43(8): 4320–4327, 1991. doi: 10.1103/PhysRevA.43.4320.

[14] A. Hantsch and U. Gross. Numerical Simulation of Falling Liquid Film Flow on a Vertical Plane by Two-Phase Lattice Boltzmann Method. *J. Engineering*, 2013: 484137, 2013. doi: 10.1155/2013/484137.

[15] X. He and G.D. Doolen. Thermodynamic Foundations of Kinetic Theory and Lattice Boltzmann Models for Multiphase Flows. *J. Statistical Physics*, 107: 309–328, 2002.

[16] X. He, Q. Zou, L.-S. Luo, and M. Dembo. Analytic solutions of simple flows and analysis of nonslip boundary conditions for the lattice Boltzmann BGK model. *Journal of Statistical Physics*, 87(1-2): 115–136, 1997.

[17] X. He, S. Chen, and G.D. Doolen. A novel thermal model for the lattice Boltzmann method in incompressible limit. *J. Computational Physics*, 146: 282–300, 1998.

[18] X. He and L.-S. Luo. Theory of the lattice Boltzmann method : From the Boltzmann equation to the lattice Boltzmann equation. *Phys. Rev. E*, 56: 6811–6818, 1997. doi: 10.1103/PhysRevE.56.6811.

[19] X. He, X. Shan, and G. D. Doolen. Discrete Boltzmann equation model for nonideal gases. *Phys. Rev. E*, 57: R13-R16, 1998. doi: 10.1103/PhysRevE.57.R13.

[20] T. Inamuro, N. Konishi, and F. Ogino. Galilean invariant model of the lattice Boltzmann method for multiphase fluid flows using free-energy approach. *Computer Physics Communications*, 129(1): 32–45, 2000.

[21] T. Inamuro, T. Ogata, S. Tajima, and N. Konishi. A lattice Boltzmann method for incompressible two-phase flows with large density differences. *J. Comp. Physics*, 198(2): 628–644, 2004.

[22] D. Jamet, D. Torres, and J.U. Brackbill. On the theory and computation of surface tension: The elimination of parasitic currents through energy conservation in the second-gradient method. *J. Computational Physics*, 182(1): 262–276, 2002. doi: DOI: 10,1006/jeph, 2002, 7165.

[23] A. Kuzmin, A.A. Mohamad, and S. Succi. Multi-relaxation time lattice Boltzmann model for multiphase flows. *Int. J. Modern Physics C*, 19 (6): 875–902, 2008.

[24] S. Leclaire, M. Reggio, and J.-Y. Trépanier. Progress and investigation on lattice Boltzmann modeling of multiple immiscible fluids or components with variable density and viscosity ratios. *J. Computational Physics*, 246: 318–342, 2013.

[25] R.A. Ledesma Aguilar. *Hydrophobicity in capillary flows. Dynamics and stability of menisci, thin films and filaments in confined geometries*. PhD thesis, Universitat de Barcelona, 2009.

[26] T. Lee and P.F. Fischer. Eliminating parasitic currents in the lattice Boltzmann equation method for nonideal gases, *Phys. Rev. E*, 74(4): 046709, 2006. doi: 10.1103/PhysRevE.74.046709.

[27] T. Lee and L. Liu. Wall boundary conditions in the lattice Boltzmann equation method for nonideal gases. *Phys. Rev. E*, 78:017702, 2008. doi:10.1103/PhysRevE.78.017702.

[28] T. Lee and L. Liu. Lattice Boltzmann simulations of micron-scale drop impact on dry surfaces. *J. Comp. Physics*, 229(20): 8045–8063, 2010.

[29] T. Lee and C.-L. Lin. A stable discretization of the lattice Boltzmann equation for simulation of incompressible two-phase flows at high density ratio. *J. Comp. Physics*, 206(1): 16-47, 2005. doi: DOI: 10.1016/j.jcp.2004.12.001.

[30] D.R. Noble, S. Chen, J.G. Georgiadis, and R.O. Buckius. A consistent hydrodynamic boundary condition for the lattice Boltzmann method. *Physics Fluids*, 7(l): 203–209, 1995. doi:10.1063/1.868767.

[31] A. Prosperetti and G. Trvggvason, editors. *Computational Methods for Multiphase Flow*. Cambridge University Press, Cambridge, 2007.

[32] T. Reis and T.N. Phillips. Lattice Boltzmann model for simulating immiscible two-phase flows. *J. Physics A*, 40(14): 4033–4053, 2007.

[33] D.H. Rothman and J.M. Keller. Immiscible cellular-automaton fluids. *J. Statistical Physics*, 52:1119-1127, 1988.

[34] M. Sbragaglia, R. Benzi, L. Biferale, S. Succi, K. Sugivama, and F. Toschi. Generalized lattice Boltzmann method with multi-range pseudopotential. *Phys. Rev. E*, 75:1–13, 2007.

[35] X. Shan and H. Chen. Lattice Boltzmann model for simulating flows with multiple phases and components. *Phys. Rev. E.*, 47:1815–1819, 1993. doi: 10.1103/PhysRevE.47.1815.

[36] C.-H. Shih, C.-L. Wu, L.-C. Chang, and C.-A. Lin. Lattice Boltzmann simulations of incompressible liquid-gas systems on partial wetting surfaces. *Philosophical Transactions of the Royal Society A: Mathematical, Physical and Engineering Sciences*, 369(1945): 2510–2518, 2011. doi: 10.1098/rsta.2011.0073.

[37] K. Sun, T. Wang, M. Jia, and G. Xiao. Evaluation of force implementation in pseudopotential-based multiphase lattice Boltzmann models. *Physica A*, 391(15): 3895–3907, 2012.

[38] M.R. Swift, W.R. Osborn, and J. M. Yeomans. Lattice Boltzmann simulation of nonideal fluids. *Phys. Rev. Lett.*, 75(5): 830–833, Jul 1995. doi: 10,1103/PhysRevLett,75,830

[39] A.J. Wagner. The origin of spurious velocities in lattice Boltzmann. *Int. J. Modern Physics B*, 17(1-2):193–196, 2003.

[40] G. Wellein, Y. Zeiser, G. Hager, and S. Donath, On the single processor performance of simple lattice Boltzmann kernels, *Comput. Math. Appl.*, 35: 910–919, 2006.

[41] Y.Y. Yan and Y.Q. Zu. A lattice Boltzmann method for incompressible two-phase flows on partial wetting surface with large density ratio. *J. Comp. Physics*, 227(l): 763–775, 2007.

[42] D. Yu, E. Mei, L.-S. Luo, and W. Shyy. Viscous flow computations with the method of lattice Boltzmann equation. *Progress in Aerospace Sciences*, 39(5): 329–367, 2003.